Research Square

Preprints are preliminary reports that have not undergone peer review.
They should not be considered conclusive, used to inform clinical practice,
or referenced by the media as validated information.

Parabolic flight-induced gravity variations initiate acute functional and transcriptional responses in cardiac organoids

Emma Yamagata Cretin

emma@alatyr.space

ALATYR

Héloïse Réthoré

ALATYR

Frank Yates

SupBiotech, Ecole d'Ingénieurs en Biotechnologies

Côme Rossary

ALATYR

Patrick Gonzalez

SupBiotech, Ecole d'Ingénieurs en Biotechnologies

Callum Burnard

SupBiotech, Ecole d'Ingénieurs en Biotechnologies

David Gosselin

ALATYR

Article

Keywords:

Posted Date: November 2nd, 2026

DOI: https://doi.org/10.21203/rs.3.rs-11060131/v1

License: This work is licensed under a Creative Commons Attribution 4.0 International License.
Read Full License

Additional Declarations: Competing interest reported. E.Y and D.G are employed by ALATYR but declare no non-financial competing interests. The remaining authors declare no financial or non-financial competing interests.

Parabolic flight-induced gravity variations initiate acute functional and transcriptional responses in cardiac organoids

Emma Yamagata Cretin[1✉], Héloïse Réthoré[1,2], Frank Yates[2,3], Côme Rossary[1,4], Patrick Gonzalez[2], Callum Burnard[2,7], David Gosselin[1]

Affiliations

[1]ALATYR, Saint-Germain-En-Laye, France.

[2]SupBiotech, Ecole d'Ingénieurs en Biotechnologies, Villejuif, France.

[3]Commissariat à l'Energie Atomique et aux Energies Alternatives (CEA), Service d'Etude des Prions et des Infections Atypiques (SEPIA), Université Paris-Saclay, Fontenay-aux-Roses, France.

[4]ISAE-SUPAERO, Toulouse, France.

[7]Université Claude Bernard Lyon 1, Laboratoire Physiopathologie et Génétique du Neurone et du Muscle-Institut NeuroMyoGène, Team « Chromatin dynamics, nuclear domains, virus », PGNM-INMG, UCBL - CNRS UMR5261 - INSERM U1315, LAbEx Dev2CAN, Faculté de Médecine et de Pharmacie, F69008, Lyon, France

✉Corresponding author. E-mail: emma@alatyr.space

ABSTRACT

Changes of gravity induce profound cardiovascular adaptations in astronauts during spaceflights. Yet the early physiological mechanisms initiating cardiac remodeling remain unclear, as most studies have focused on long-duration spaceflight adaptations. Here, we investigated early functional and molecular responses using three-dimensional cardiac organoids derived from mouse embryonic stem cells exposed to altered gravity during the 69th CNES (Centre National d'Etudes Spatiales) parabolic flight campaign. Cardiac organoids were exposed to 31 consecutive parabola comprising repeated microgravity and hypergravity phases, followed by immediate functional and transcriptomic analyses after the flight. In this study, parabolic flight-induced gravity variations were associated with maturation-dependent adaptations, increased cardiac beating rate and modified calcium dynamics. Transcriptomic

analyses revealed modifications of gene expressions involved in calcium homeostasis, mitochondrial function and stress-related pathways, including upregulation of *S100g*, *Ifi27l2a*, *Prelid2*, *Spink1* and *Apom*. Together, these findings support the use of cardiac organoids and parabolic flight as a complementary research platform to investigate early functional and molecular mechanisms of cardiac adaptation to gravity variation.

INTRODUCTION

Human spaceflights have highlighted gravity as a major environmental force of human and mammalian evolution on Earth[1–3]. Indeed, exposure to reduced gravitational loading, defined as microgravity, is associated with a range of physiological adaptations observed in astronauts during their space missions. One of the earliest physiological modifications under microgravity is the redistribution of body fluids from the lower extremities and abdomen toward the heart and the head. This major fluid redistribution directly affects the neurological and cardiovascular system[4,5]. Progressively, astronauts display brain tissue shift and cerebrospinal fluid redistribution associated with intracranial hypertension, spaceflight associated neuro-ocular syndrome (SANS) and vestibular disturbance described as space motion sickness (SMS)[6–8]. Fluid shift also induces a decrease in circulating blood volume of 7-15%, contributing to a decrease in global pressure, a reduction in cardiac stroke volume[9] and cardiovascular deconditioning[10,11]. In addition, microgravity alters mechanosensitive systems leading to musculoskeletal deficiencies, categorized as osteoporosis and sarcopenia[12,13], and dysfunctions of the innate and adaptive immune system[14–17].

Cardiovascular monitoring of astronauts during spaceflight revealed a significantly increased incidence of arrhythmias, including premature atrial and ventricular contractions, atrial fibrillation and episodes of ventricular tachycardia[18]. Cardiac remodeling is also rapidly observed with vascular dysfunctions and cardiac atrophy reported in 80% of astronauts[10,11,19]. All these microgravity adaptations contribute to reduced exercise capabilities and post-flight orthostatic intolerance upon astronauts return to Earth[20].

In parallel, long-term experiments on cardiac cells or tissues conducted aboard the International Space Station (ISS) have provided insight into spaceflight-induced

cellular and molecular responses. Human cardiomyocytes derived from induced pluripotent stem cells (iPSCs) were cultured for 40 days aboard the ISS and revealed changes in calcium handling and upregulation of genes associated with reactive oxygen species, cellular stress responses and mitochondrial metabolism[21]. Studies using human adult and neonatal cardiovascular progenitor cells (CPCs) cultured on the ISS for 30 days demonstrated several unique maturation-dependent effects of spaceflight, including modifications in stemness, senescence, proliferation and survival signaling pathways[22]. Additional experiments using cardiac progenitor spheroids exposed to spaceflight conditions for 21 days aboard the ISS further indicated an increased expression of genes related to cell proliferation, cardiac differentiation and cardiac function[23]. Finally, engineered heart tissues (EHTs) from hiPSCs-derived cardiomyocytes were cultured up to 30 days on the ISS and exhibited increased sign of arrhythmias and mitochondrial damage associated with upregulation of pathways linked to metabolic disorders, heart failure, oxidative stress and inflammation[24]. Taken together, these studies suggest that spaceflight-induced responses vary according to the complexity (cellular versus tissue-level organization) and maturation state of the experimental model, highlighting the need for more physiologically relevant models to study cardiac adaptations to spaceflight, such as cardiac organoids. In addition, these studies have primarily focused on the effects of long-term exposure to microgravity (>21 days), limiting insight into early and acute functional and molecular responses. Yet, characterizing the onset of the cardiovascular response to altered gravity may be critical to elucidate early molecular pathways influencing the progression of cardiovascular alterations during spaceflight.

Parabolic flight, a ground-based spaceflight analog[25], have been previously used to study the immediate effect of altered gravity on the cardiovascular system[26]. During the 29th European Space Agency (ESA) parabolic flight campaign, the heart rate variability (HRV) of seven healthy volunteers was recorded using electrocardiogram (ECG), demonstrating a tendency to higher HRV during the microgravity phases[27]. A separate study conducted during the 31st German space agency (DLR) parabolic flight campaign analyzed the blood levels of heart failure biomarkers in fourteen healthy volunteers and observed an influence of gravity variations on cardiac stress and calcium homeostasis[28]. More recently, the beating rate of human iPSCs-derived cardiomyocytes were monitored after each parabola during the 66th ESA parabolic

flight campaign and displayed a progressive beating rate acceleration, reaching up to 40% increase after 15 parabolas[26]. This functional modulation was suggested to involve the L-type Calcium Channel activity[26]. Altogether, these findings highlighted parabolic flight as an interesting ground-based analog to examine the onset of cardiac adaptations to gravity variations and suggested rapid cardiac beating rate and calcium fluxes modifications following parabolic-flight induced gravity modifications.

In this study, we generated cardiac organoids derived from mouse embryonic stem cells and exposed them to parabolic flights at different stages of maturation. Spontaneous cardiac contractility, calcium dynamics and transcriptomics were immediately assessed after the flights. By combining functional and molecular analyses, we aimed to determine whether acute exposure to parabolic flight-induced repeated microgravity and hypergravity cycles displayed measurable functional changes associated with novel transcriptomics signature in cardiac organoids.

RESULTS

Generation of mouse cardiac organoids (COs) for parabolic flights

We started by assembling mouse embryonic stem cells (mESCs) into embryoid bodies (EBs) in ultra-low attachment 96-well plates for 72h incubation prior to cardiac induction (Figure 1.a). Mesoderm and cardiac differentiation were induced by FGF4, in an adaptation of a previously described protocol[29,30]. Brightfield imaging of the cardiac organoids (COs) showed a significant morphological evolution over the course of differentiation (Figure 1.b). By day 3, COs reached a mean diameter of 1157 µm and started showing sphere buds (Sb) (Figure 1.c). By day 7, proliferative growth slowed down as COs reached a maximum mean diameter of 1368 µm and differentiation progressed toward cardiac maturation, with morphology transitioning toward beating heart tube-like (HT) structures and chamber formation (CF), as described previously[29].

The efficiency of cardiac differentiation was evaluated using time-course flow cytometry analysis with pluripotency (OCT3/4), fibroblasts (VIMENTIN), mesoderm (EOMES), sarcomere (ACTN2), and cardiomyocyte-specific (TNNT2) markers. At day 3, 19.61% of cells expressed the mesodermal marker EOMES and 50.56% the sarcomere protein ACTN2, indicating the presence of progenitors and the initiation of

sarcomere organization (Figure 1.d). By day 7, ACTN2 and TNNT2 expressions increased to 34.4% and 11.9%, respectively, and reached 77.84% and 68,31% by day 9, demonstrating a rapid cardiomyocyte maturation. Spontaneous contractions were observed from day 3, with 22.9% of COs exhibiting visible beating (Figure 2.a). The proportion of beating organoids continues increasing over time, reaching 45.8% on day 7 (Supplementary Movie 1) and 83.8% by day 9 (Supplementary Movie 2). Their beating frequency remained stable with a mean of 54 beating per minute, staying in the quality control range of 30 – 90 bpm previously recommended[31] (Figure 2.b).

Consistent with these observations, live calcium fluxes imaging revealed regular Ca^{2+} transients characteristic of functional cardiac tissue at days 7 and 9 (Figure 2.c and 2.d, Supplementary Movie 3 and Supplementary Movie 4). As well as comparable Ca^{2+} amplitude (Figure 2.e), transient decay tau (Figure 2.f), and frequency (Figure 2.g).

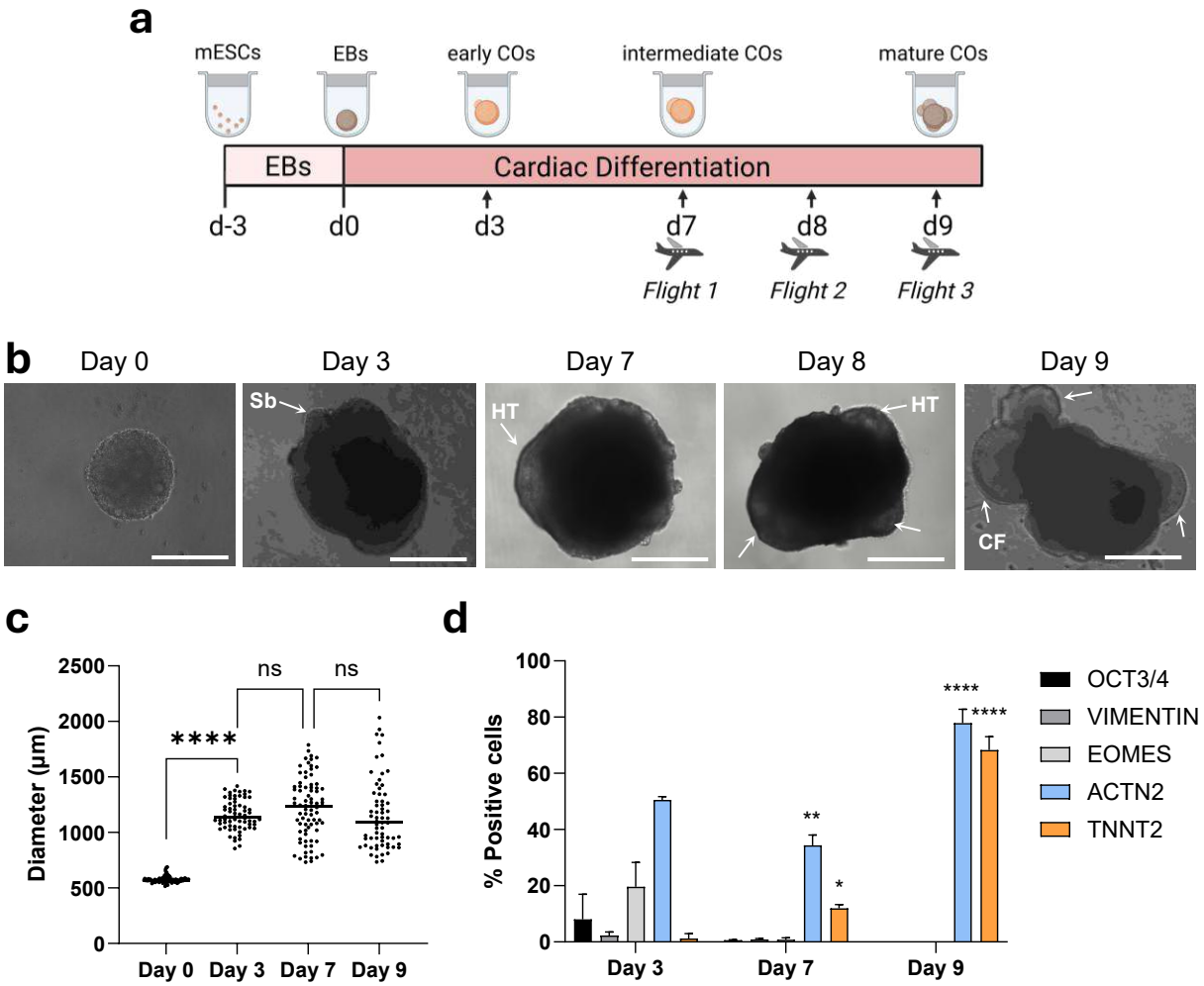


Figure 1. Generation of mouse cardiac organoids for the parabolic flight.

a. Schematic overview of the differentiation workflow used for generating cardiac organoids (COs). At day 7, 8 and 9 COs were exposed to parabolic flight. Created using BioRender.com.

b. Brightfield images of COs through the 9-days culture period. One representative organoid is shown for each condition. Arrows indicate sphere buds (Sb), heart tube-like (HT) and chamber formation (CF) morphology. Scale bar = 500µm.

c. Quantification of COs diameter at day 0, 3, 7 and 9 (data representative of 65-106 independent organoids per conditions across three independent experiments, Median, Ordinary one-way ANOVA; **** p-value<0.0001, ns: not significant).

d. Time course flow cytometry analysis of COs at day 3, 7 and 9 with pluripotency (OCT3/4), fibroblasts (VIMENTIN), mesoderm (EOMES), sarcomere (ACTN2) and cardiomyocyte-specific (TNNT2) markers (data representative of 8 independent organoids per conditions across three independent experiments, Mean ± SD, Ordinary one-way ANOVA; * p-value<0.05, ** p-value<0.01, **** p-value<0.0001).

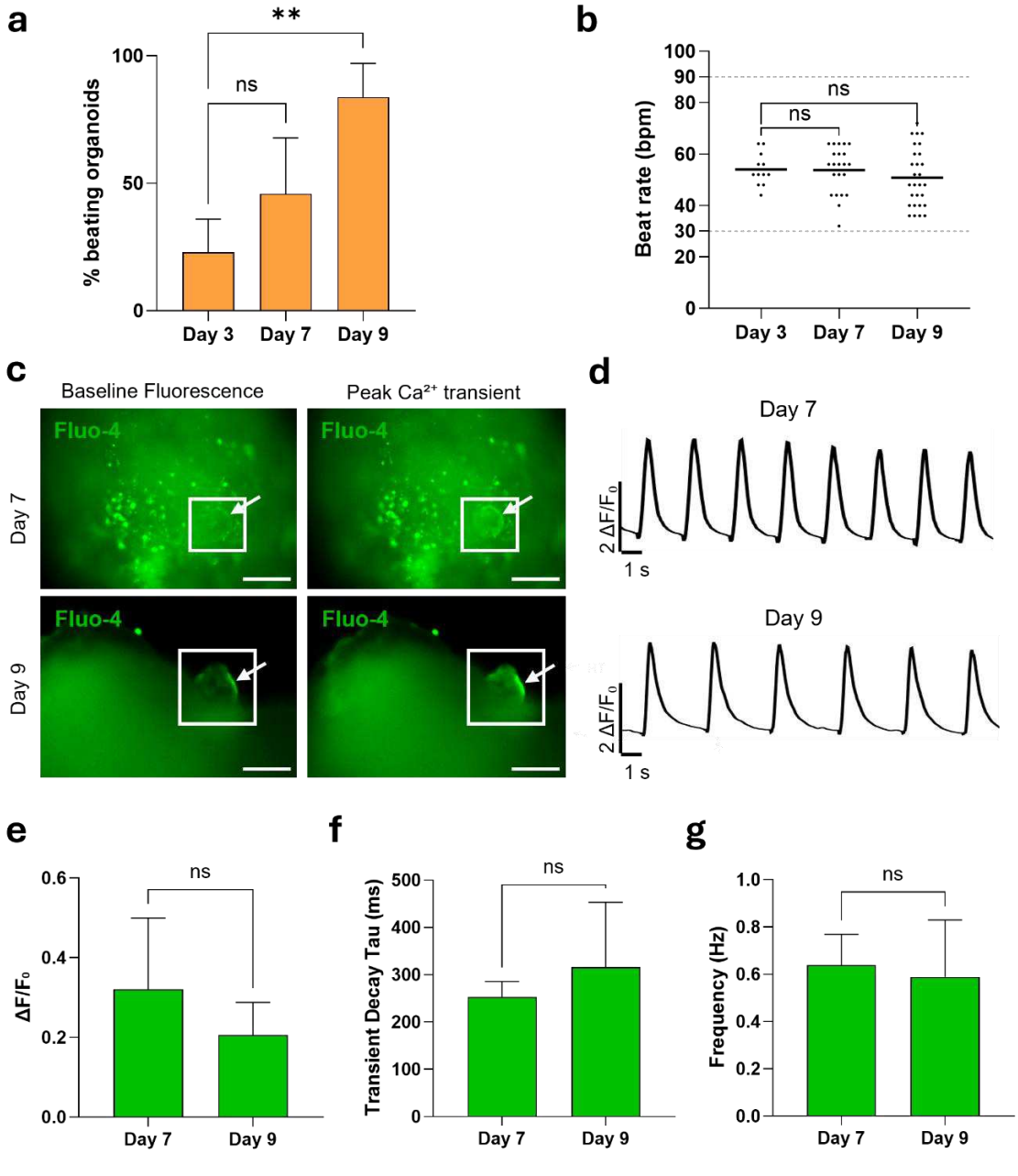


Figure 2. Cardiac organoids functional characterization prior to parabolic flights.

a. Percentage of organoids visibly beating under brightfield microscopy at day 3, 7 and 9 (data representative of 16 independent organoids per condition across three independent experiments, Mean ± SD, Ordinary one-way ANOVA, **p-value<0.01, ns: not significant).

b. Beating frequency in beats per minute (bpm) of organoids on day 3, 7 and 9. Grey dashed line corresponds to the quality control range of 30-90 bpm (data representative of 12-28 independent organoids per conditions across three independent experiments, Mean, Ordinary one-way ANOVA, ns: not significant).

c. Representative Fluo-4 fluorescence images of organoids at day 7 and day 9 showing baseline intracellular Ca^{2+} levels (white box, left) and peak Ca^{2+} transient (white box, right) during spontaneous calcium fluxes. 1 representative organoid is shown for each condition. Scale bar = 500 µm.

d. Representative traces of calcium transient of COs on day 7 and day 9.

e-f-g. Quantification of Ca^{2+} transient traces with $\Delta F/F_0$ (**e**), transient decay Tau (**f**) and frequency (**g**) of COs at day 8 and 9 (data representative of 4 independent organoids per conditions across three independent experiments, Mean ± SD, Welch's t test, ns: not significant).

Functional analyses of cardiac organoids exposed to parabolic flights

The cardiac organoids were flown on three independent parabolic flights conducted on consecutive days at different maturation stages: day 7 on Flight 1, day 8 on Flight 2, and day 9 on Flight 3. The parabolic flight campaign was sponsored by the Centre National d'Études Spatiales (CNES) and operated by Novespace (Bordeaux, France) with an Airbus A310. Before each flight, the COs were divided into two groups: a 1 g control maintained on the ground under standard Earth gravity conditions, and a flight group, exposed to gravity variations across 31 parabolas during the parabolic flight. Each parabola consisted of three phases: first, the airplane was pulled up for about 24 s with full thrust. During this hypergravity phase, the COs were subjected to an acceleration of approximately 1.8 g. Then, the airplane followed a parabolic trajectory with the engine thrust reduced to the minimum, entering a free-fall phase for approximately 22 s during which the COs were exposed to microgravity. Finally, the airplane was pulled out of the parabola through a last hypergravity phase of approximately 1.8 g for 22 s (Figure 3).

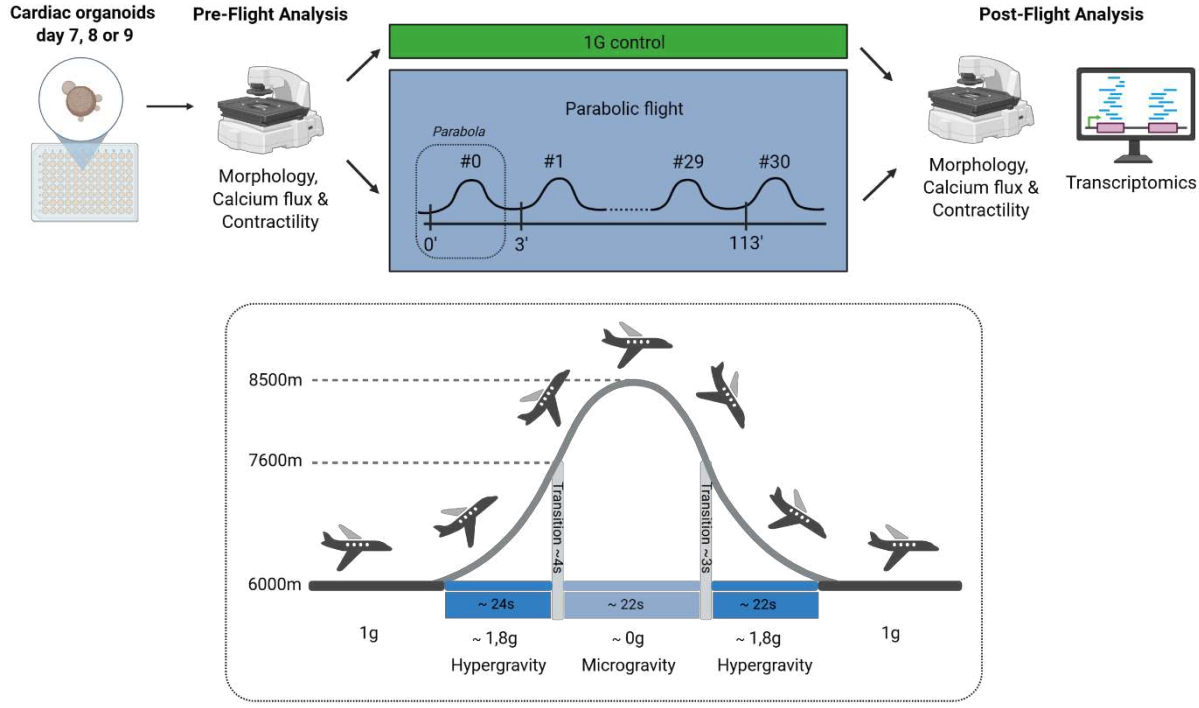


Figure 3. Overview of parabolic flight experiments.
Schematic overview of the parabolic flight experiment design. The morphology, contractility and calcium flux of COs on day 7 (Flight 1), 8 (Flight 2) or 9 (Flight 3) were assessed before the flight. COs were then divided into two groups: the first group stayed on the ground as 1g control, while the second group was exposed to parabolic flight comprising 31 parabolas, each consisting of a first hypergravity phase (~1.8g) for 24s, followed by microgravity (~0g) for 22s and a final hypergravity period (~1.8g) for 22s. Immediately after the flight, COs morphology, contractility and calcium fluxes were measured again and others were immediately frozen for transcriptomics analysis. Created using BioRender.com.

Prior to the flights and immediately after landing, COs morphology, contractility and calcium fluxes were recorded to analyse the acute effect of gravity alteration on cardiac function.

COs had similar morphology before and after the flights (Figure 4.a), with a relative diameter (Δdiameter: post-flight/pre-flight) around 0.98 across all flights (Figure 4.b). Interestingly, a significant increase in contractility rate was observed following Flight 2 and 3, with a relative beating per minute (Δbpm: post-flight/pre-flight) increasing by 28.44% in day 8 organoids and by 32.93% in day 9 organoids (Figure 4.c). However, the relative beating per minute was unchanged for early COs at day 7 after Flight 1.

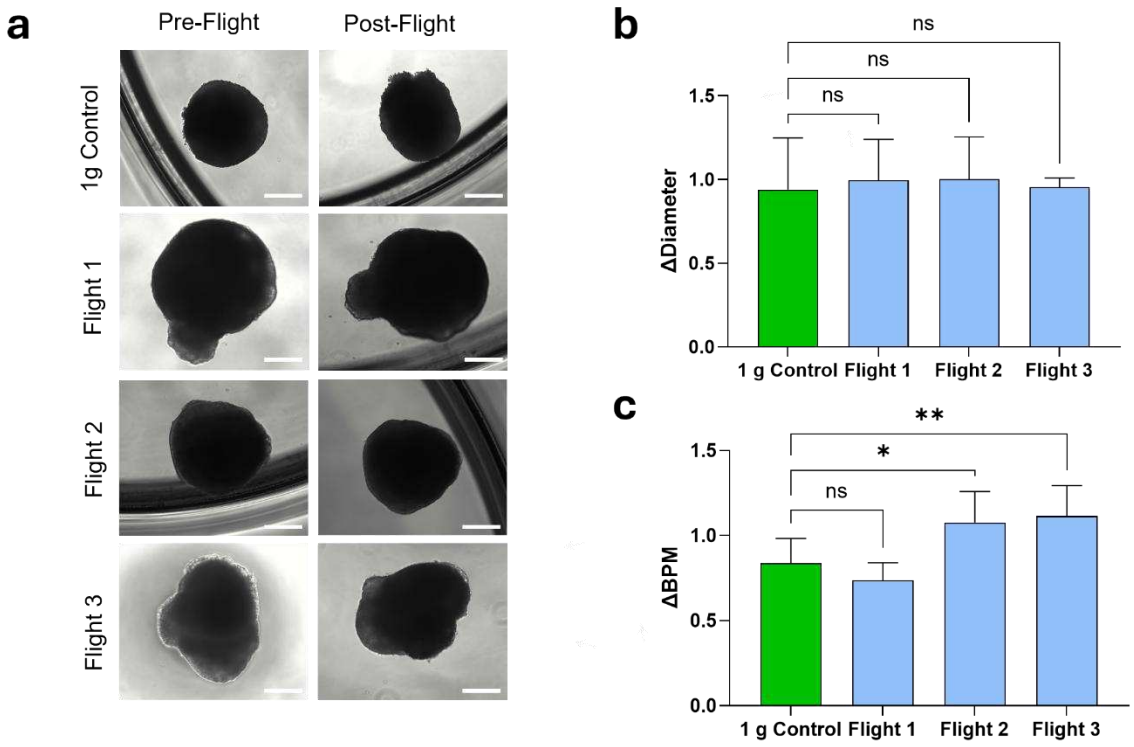


Figure 1. Effects of parabolic flights on cardiac organoids morphology and contractility.
a. Brightfield images of COs before (Pre-Flight) and after (Post-Flight) the parabolic flight, and corresponding 1g controls. One representative organoid is shown for each condition. Scale bar = 500µm.
b. Quantification of organoid diameter (expressed as Δdiameter: post-flight diameter/pre-flight diameter) following parabolic flight, and corresponding 1g control (data representative of 5-11 independent organoids per conditions across three independent experiments, Mean ± SD, Ordinary one-way ANOVA, ns: not significant).
c. Quantification of organoid contraction at day 7 (Flight 1), day 8 (Flight 2) and day 9 (Flight 3). COs contractility is expressed as ΔBPM (post-flight beating per minute/pre-flight beating per minute) following parabolic flight, and corresponding 1g control (data representative of 5-16 independent organoids per conditions across three independent experiments, Mean ± SD, Ordinary one-way ANOVA, *p-value<0.05, **p-value<0.01, ns: not significant).

Consistent with the contractile modification at later maturation stages, calcium transient traces revealed modified Ca^{2+} handling properties of cardiac organoids exposed to Flights 2 and 3 (Figure 5.a). Organoids at day 8 and day 9 exhibited a significant increase in Ca^{2+} transient amplitude (Figure 5.b), associated with an increase in transient decay tau (Figure 5.c) but comparable frequency (Figure 5.d). Again, no difference in calcium dynamics was observed in early COs at day 7 following Flight 1.

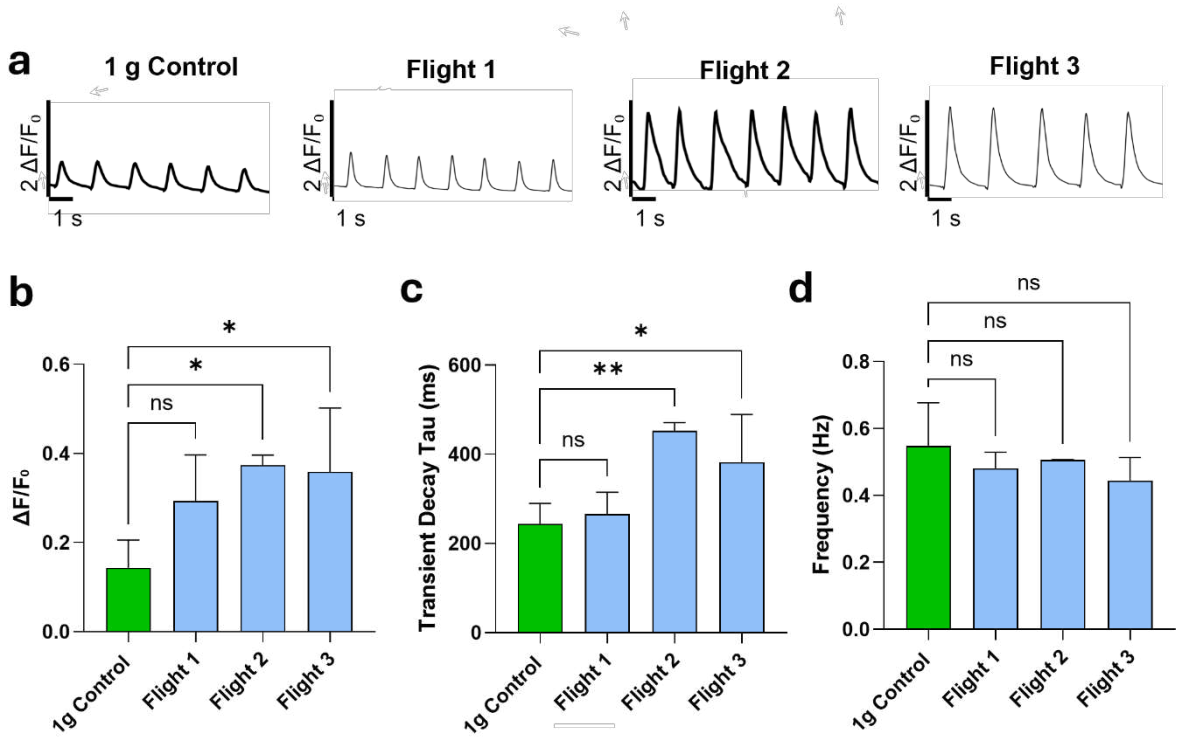


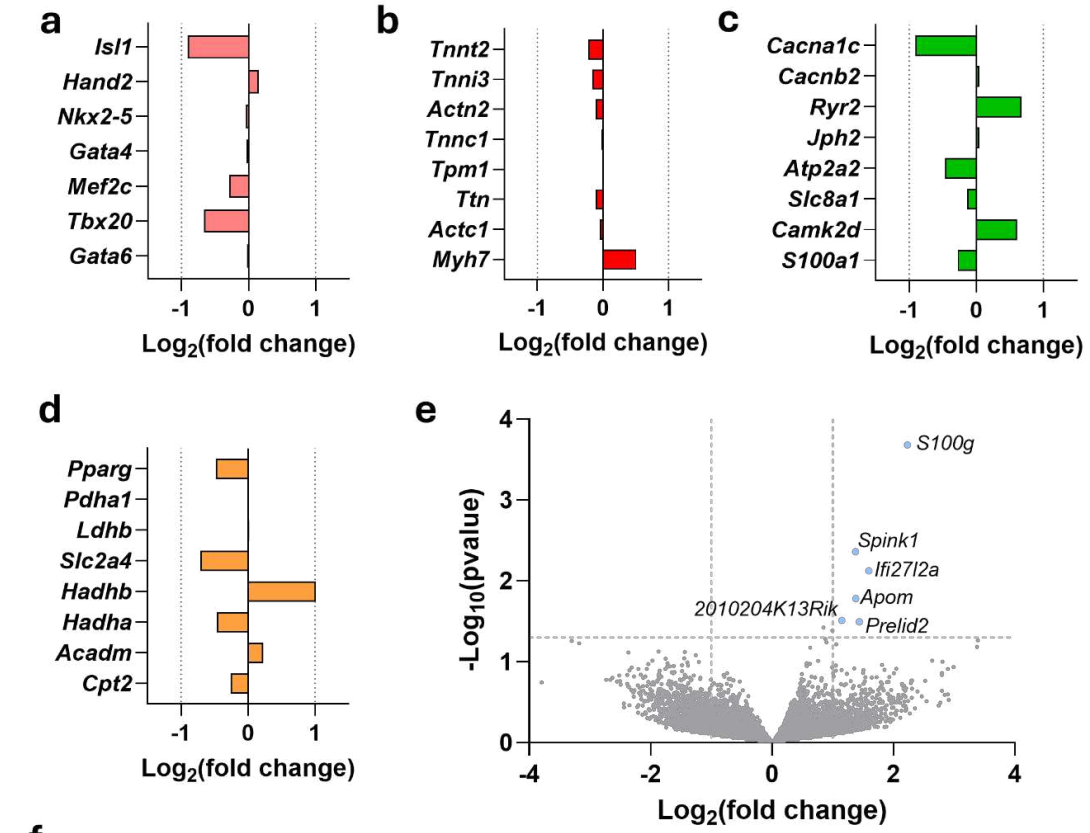
Figure 2. Effects of parabolic flights on cardiac organoids calcium fluxes.
a. Representative traces of calcium transient of COs at day 7 (Flight 1), day 8 (Flight 2) and day 9 (Flight 3).
b-c-d. Quantification of Ca^{2+} transient traces with $\Delta F/F_0$ **(b),** transient decay Tau **(c)** and frequency **(d)** of COs at day 7 (Flight 1), day 8 (Flight 2) and day 9 (Flight 3), and corresponding 1g control (data representative of 2-8 independent organoids per flight or 1g control, Mean ± SD, Ordinary one-way ANOVA, *p-value<0.05, **p-value<0.01, ns: not significant).

Transcriptomics remodeling in cardiac organoids following gravity variations during parabolic flights

After landing, mouse cardiac organoids exposed to parabolic flight, together with their corresponding 1 g control, were immediately frozen for transcriptomics analysis. In order to capture global acute transcriptional response to parabolic flight, in a maturation-stage independent manner, total RNA sequencing was performed on

pooled cardiac organoids collected at days 7, 8 and 9. Based on the previously observed modifications in contractility and calcium flux following parabolic flight exposure, we first examined the expression of genes encoding cardiac transcription factors (Figure 6.a) and genes related to cardiac contractility (Figure 6.b), calcium handling (Figure 6.c), and cardiac metabolism (Figure 6.d). No differences in expression were detected for any of those genes, indicating that parabolic flight did not induce immediate transcriptional changes in genes known to be involved with cardiac contractility and metabolism or calcium dynamics. We therefore focused on the global transcriptomic dataset, which revealed six genes upregulated in response to repeated hypergravity and microgravity exposure during parabolic flight (p-value< 0.05 and $\log_2$(fold change)> 1; Figure 6.e). Interestingly, the most upregulated gene was *S100g* (p-value=0.00021, $\log_2$(fold change)=2.23; Figure 6.f-g), which encodes a cytosolic calcium-binding protein involved in intracellular calcium buffering and signaling[32]. While several members of the S100 protein family have previously been identified as markers of microgravity exposure in astronaut serum, *S100g* has not, to our knowledge, been reported in this context[33]. The second most upregulated gene was *Ifi27l2a* (p-value=0.007, $\log_2$(fold change)=1.59), an interferon-inducible gene associated with inflammation and mitochondrial ROS production[34]. While inflammation and mitochondrial dysfunctions have been widely reported in response to microgravity[35], *Ifi27l2a* has not been reported in previous microgravity studies. In parallel, *Prelid2*, a gene encoding a mitochondrial lipid transfer protein involved in phospholipid trafficking to the inner mitochondrial membrane, was also upregulated (p-value=0.032, $\log_2$(fold change)=1.44). Similarly, modifications in *Prelid2* expression have never been reported in previous microgravity or gravity variations exposure studies. *Apom*, encoding the apolipoprotein M, a lipid transport protein and carrier of sphingosine-1-phosphate (S1P) implicated in immune and inflammatory response[36], showed increased expression following parabolic flight exposure (p-value=0.016, $\log_2$(fold change)=1.38). Although *Apoa1*, another apolipoprotein family member, has been reported to be elevated in astronaut serum after prolonged spaceflight[33], *Apom*, has not been identified yet under these conditions. Elevated transcript level was detected for *Spink1* (p-value=0.004, $\log_2$(fold change)=1.37), a serine protease inhibitor previously reported to be involved in chronic pancreatitis, pancreatic cancer and upregulated in ischemic heart disease[37,38]. Finally, *2010204K13Rik*, a gene with currently uncharacterized biological function, was also found upregulated (p-

value=0.03, log_2(fold change)=1.15). These results suggest that parabolic flight-induced gravity variations is associated with an acute transcriptional response through the specific upregulation of genes involved in calcium homeostasis, stress response, lipid transport, and mitochondria.



f

Gene Name	Function
S100g (S100 calcium binding protein G)	Ca^{2+} homeostasis
Ifi27l2a (interferon, alpha-inducible protein 27 like 2A)	Stess response, apoptosis-related
Prelid2 (PRELI domain containing 2)	Mitochondrial phospholipd transfer
Apom (apolipoprotein M)	Lipid signaling, cell survival
Spink1 (serine peptidase inhibitor, Kazal type 1)	Stress response, tissue protection
2010204K13Rik (RIKEN cDNA 2010204K13 gene)	Unknown

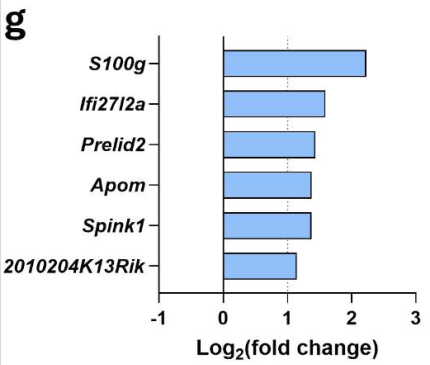


Figure 6. RNA-sequencing analysis of COs exposed to parabolic flights.
a-b-c-d. Log2(fold change) of cardiac transcription factors **(a)**, genes related to cardiac contractility **(b)**, calcium handling **(c)** and cardiac metabolism **(d)**.
e. Volcano plot illustrating differential gene expression between parabolic flights-exposed COs and 1g ground controls. Genes with p-value < 0.05 and Log_2(fold change) > 1 are represented with red dots. The x-axis represents Log_2(fold change) and y-axis the $-Log_{10}$(p-value unadjusted).
f. Table summarizing the main cellular functions of the 6 genes upregulated in cardiac organoids exposed to parabolic flight compared to the 1g ground control.
g. Log2(fold change) of the 6 upregulated genes following parabolic flight.

DISCUSSION

Cardiovascular adaptations during spaceflight are consistently reported in both low Earth orbit and deep-space missions, including the Apollo lunar missions[19,39]. Previous studies report the effects of long-term missions on cardiac tissue, progenitors, or cardiomyocytes, describing functional and metabolic remodeling following weeks or months of microgravity exposure aboard the ISS[21,23,24,40]. Yet the early mechanisms modulating cardiovascular physiology under microgravity remain unclear. Short-duration studies, using parabolic flight, demonstrated rapid cardiac response to gravity variations, with higher heart rate variability during the microgravity phases[27] and rapid modulation of cardiomyocytes beating rate[26].

In this study, we focused on acute cardiac functional and molecular responses using cardiac organoids derived from mouse embryonic stem cells exposed to parabolic flights. We used three-dimensional cardiac organoids displaying spontaneous beating and coordinated calcium dynamics to better simulate *in vivo* cardiac function. Unlike previous studies, we analyzed cardiac responses following exposure to the full parabolic sequences, including repeated microgravity and hypergravity cycles, to assess the global effect of altered gravity exposure[26,41]. We observed that parabolic flight induces cardiac functional adaptations in a maturation-dependent manner. Indeed, while organoids at day 7 of differentiation showed no significant functional modifications, organoids at day 8 and 9 exhibited immediate significant increase in beating rate, calcium transient amplitude, and decay Tau. These findings were consistent with previous studies showing maturation-dependent cardiac adaptation during spaceflight using human adult and neonatal cardiovascular progenitor cells[22]. The immediate increase in beating rate and transient decay Tau was also in accordance with previous observations in human cardiomyocytes exposed to parabolic flight or long-term spaceflight, respectively[26,42]. In contrast, cardiac organoid morphology remained unchanged following the parabolic flight, suggesting that the cardiac atrophy reported during spaceflight reflects long-term remodeling processes[19].

Despite the immediate functional adaptations observed in mature organoids, transcriptomics analysis did not reveal modifications in the expression of genes known to be associated with cardiac contractility, calcium handling or cardiac metabolism. However, a novel set of six genes was identified as upregulated following parabolic exposure, suggesting a potential transcriptomic signature associated with the acute

response to combined microgravity and hypergravity conditions. In particular, *S100g*, encoding a calcium-binding protein involved in intracellular calcium buffering, showed the strongest upregulation. Previous serum proteomic analyses of astronauts following long-duration spaceflight has identified an increase in proteins from the same S100 family, including S100A8 and S100A12, suggesting a compensatory mechanism aimed at maintaining calcium homeostasis[33]. However, S100G was never, to our knowledge, previously associated with gravity variations.

Genes associated with mitochondrial function and stress responses, *Ifi27l2a* and *Prelid2,* were also upregulated, indicating early inflammation and acute mitochondrial response that are consistent with stress response observed after long-term spaceflight exposure[24,35]. In addition, the upregulation of *Apom*, a gene encoding a lipid transport protein involved in sphingosine-1-phosphate signaling, further highlights the immediate lipid-mediated stress and inflammatory responses to altered gravity. While inflammation, oxidative stress, and mitochondrial dysfunction have been widely reported following long-term spaceflight, the present results suggest that these pathways may be activated rapidly even after short-duration exposure and unveil novel candidate genes potentially involved in the acute adaptation associated with parabolic flight-induced gravity variations [35,43,44].

However, the interpretation of these observations should consider several limitations. Due to operational constraints associated with human-derived cells handling during parabolic flight experiments, an alternative model was implemented. While human cardiac organoids derived from induced pluripotent stem cells would offer direct translational relevance, mouse embryonic stem cell-derived cardiac organoids constitute a robust and widely used model in space biology. This model enables the investigation of conserved cellular responses to altered gravity conditions and provides insights into the signaling pathways governing mechanotransduction and tissue organization under mechanical constraint[41,45–47]. Another important limitation of this study is that the parabolic flight campaign design does not allow dissociation of the specific contribution of gravity transitions from other flight-associated factors, including vibrations, aircraft acceleration and other operational constraints. In the absence of an in-flight non-parabolic control condition, the observed functional and transcriptional responses should therefore be interpreted as associated with exposure to parabolic flight-induced gravity variations rather than attributed exclusively to altered gravity

itself. In this study, we decided to capture global acute responses to microgravity and hypergravity cycles and therefore not distinguish microgravity-specific effects. In addition, our experimental setup does not take into account other spaceflight-associated stressors known to contribute to cardiovascular alterations, such as radiations[48]. Therefore, parabolic flight experiments can not substitute for spaceflight studies but should be viewed as a complementary platform to investigate the onset of gravity variations-induced effects[49,50]. Our transcriptomics analyses were performed on pooled cardiac organoids at different maturation stages to assess the general acute response to altered gravity. While this approach identified early global transcriptional changes, further studies with samples at different maturation stages will be necessary to refine those findings. Furthermore, the limited number of differentially expressed genes may reflect rapid and acute cellular responses, potentially involving remodeling at the proteomic or post-translational level. In this context, proteomic analyses may provide complementary insights. However, it is also possible that broader transcriptional changes may emerge at later time points, reflecting longer-term adaptive processes that could be addressed in future parabolic flight studies.

Our study demonstrated that exposure to parabolic flight-induced gravity variations, through repeated microgravity and hypergravity phases, induces an acute and maturation-dependent functional adaptation in cardiac organoids, associated with a transcriptional remodeling involving calcium homeostasis, mitochondrial function, and stress-related pathways. In addition, this work highlights the value of organoids as a physiologically relevant model and parabolic flights as an important complementary platform to investigate early functional and molecular mechanisms of spaceflight adaptations.

METHODS

Mouse embryonic stem cell culture and maintenance

The mouse Embryonic Stem Cell (mESC) line ES-E14TG2 was purchased from ATCC (CRL-1821). The mESCs were cultured on irradiated Mouse Embryonic Fibroblasts (MEFs) feeder layer (A34181, FisherScientific) in DMEM High Glucose (D5796, Merck) supplemented with 10% FBS (17974731, FisherScientific), 1mM Pyruvate (S8636, Merck), 100µM β-mercaptoethanol (11508916, FisherScientific), 100U/mL

Penicillin/100µg/mL Streptomycin (P4333, Merck) and 1000 units/mL LIF (ESG1107, Merck) in a 5% CO_2 atmosphere at 37°C.

Self-assembling cardiac organoid differentiation

mESCs were grown to 60% confluency on feeder layer and dissociated using Trypsin-EDTA 0.25% (T4049, Merck) to obtain a single cell solution. The trypsinized mESCs were then seeded into six-well plates previously coated with 0.2% gelatin (G1393, Merck) and incubated at 37°C for 45 min to separate the mESCs from the MEFs feeder layer. Floating mESCs were collected and centrifuged at 1000 rpm for 5min. For Embryoid Bodies (EB) formation, 2000 mESCs were seeded onto each well of a U-bottomed 96-well plate (CLS7007, Merck) in 200µL of EB medium (Knockout DMEM (10389172, FisherScientific) supplemented with 20% FBS (17974731, FisherScientific), 100 µM β-mercaptoethanol (11508916, FisherScientific), 1× NEAA (12084947, FisherScientific), 1× EmbryoMax Nucleoside (ES-008-D, Merck), 1× P/S/Glutamine (G6784, Merck)) and incubated at 37°C and 5% CO2 for 3 days. To start cardiac differentiation, EBs were incubated with cardiac differentiation media (DMEM/F12 medium (11574546, FisherScientific) supplemented with 20% KSR (10829220, FisherScientific), 1 mM sodium pyruvate (S8636, Merck), 100 µM β-mercaptoethanol (11508916, FisherScientific) , 2 mM L-glutamine (G7513, FisherScientific), 1× P/S, 60 ng/ml progesterone (P6149, Merck), 30 ng/ml β-estradiol (E2257, Merck), 5 µg/ml insulin (I6634, Merck), 20 µg/ml transferrin (T8158, Merck), 30 nM selenite (S9133, Merck) and 45ng/ml FGF4 (235-F4, R&D systems)) for 9 days at 37 °C and 5% CO2. Cardiac differentiation medium was replaced at day 3, day 5 and day 7. The cardiac organoids were collected at different timepoint for further analysis.

AI-based Morphology Image Analysis

The morphology algorithm was implemented in Python and developed entirely in-house using Meta's Segment Anything Model (SAM) and the NumPy library. First, brightfield images acquired in .tiff were automatically converted to .png format for later processing. For each dataset, images were displayed in an interactive window, where

the user specified the microscope magnification and manually selected the organoid of interest. Segmentation of each selected organoid was performed using SAM. From the contours, the area, perimeter, circularity and equivalent perimeter was calculated. At the end of the analysis, a Microsoft Excel-compatible results.csv file was generated, containing the quantitative measurements associated with each organoid for each image.

Flow cytometry

Cardiac organoids were collected on day 3, day 7 and day 9 to monitor the efficiency of cardiac differentiation. For each sample, twelve organoids were pooled and dissociated using TryPLE Express (10718463, FisherScientific) for 10 min at 37°C followed by vigorous pipetting. Cells were washed once with PBS (15326239, FisherScientific), resuspended at $1x10^6$ cells/mL in PBS and incubated with Viobility™ 405/452 Fixable Dye (130-130-403, Miltenyi Biotec) for 10 min at room temperature (RT) following manufacturer's instructions. Cells were then fixed in 4% paraformaldehyde (15424389, FisherScientific) for 20 min at RT, washed once with PBS and permeabilized with 0.1% Triton X-100 (93443, Merck) in PBS for 20 min at RT. Permeabilized cells were incubated for 2h at 4°C with the following antibodies diluted in 5% FBS-PBS: the pluripotency marker OCT3/4 (130-123-318, Miltenyi Biotec, dilution 1:50), the fibroblast marker Vimentin (130-118-497, Miltenyi Biotec, dilution 1:50), the mesoderm marker EOMES (130-123-819, Miltenyi Biotec, dilution 1:50), the cardiomyocyte marker cardiac Troponin T (130-119-674, Miltenyi Biotec, dilution 1:50), and the sarcomere marker alpha-actinin 2 (130-119-806, MitltenyiBiotec, dilution 1:50). The cells were finally washed twice with PBS and analyzed on a MACSQuant X flow cytometer (Miltenyi Biotec). All samples were processed and analyzed using identical instrument setting and gating strategies.

Calcium Imaging

Cardiac organoids were treated with Fluo-4 calcium imaging probe (15445300, FisherScientific) in calcium-free PBS for 15 min at 37 °C and 5% CO2 and 15 min at room temperature following the manufacturer's instructions. Organoids were washed

once with Tyrode's solution and calcium fluxes were recorded using an EVOS M5000 (ThermoFisher) using a 10x objective. For the parabolic flight experiments, calcium fluxes were recorded before the flight using an EVOS M3000 with a 10x objective and immediately transported inside the plane for the flight experiment. After the flight, calcium fluxes were recorded again under identical conditions to assess the immediate impact of altered gravity. A control plate (1 g control) was prepared in the exact same conditions, subjected to normal terrestrial gravity for the same duration and recorded in the same way.

Calcium Fluxes Analysis

Calcium fluorescence fluxes were analysed using an in-house algorithm implemented in Python, based on the NumPy library, the find_peaks and curve_fit functions from the scipy.signal library. The analysis consisted of two sequential steps: first, the automated identification of the region of interest (ROI) corresponding to the area exhibiting the highest calcium flux signal, followed by the quantitative analysis of the fluorescence within this ROI.

For ROI identification, each video frame was partitioned into a regular grid of 30 × 30 spatial tiles. For each tile and each frame, the green channel of the RGB image was extracted, and the mean fluorescence intensity was computed, yielding a fluorescence time series associated with each tile. Temporal variability was quantified for each tile using a variability score defined as 100 × (variance/mean) of the fluorescence signal (this mean-normalization removes bias due to absolute brightness differences between cells). Variability scores were normalized across tiles, and the tile exhibiting the maximum score was identified. Starting from this tile, a depth-first region-growing procedure was applied, iteratively aggregating spatially connected neighboring tiles whose variability score remained within 20% of the maximum value. The final ROI was defined as the bounding box enclosing all selected tiles. In addition to this automatic procedure, a manual mode was also implemented, allowing the user to directly select the ROI.

Following ROI identification, the corresponding region was extracted from the video, and the next analyses were restricted to this area. For each frame, the mean green-channel fluorescence intensity within the ROI was computed, resulting in a one-dimensional fluorescence trace. Peaks were identified on this trace using the

find_peaks function from the scipy.signal library. Based on this, the average event frequency (f_0), the variability of inter-event intervals (Δf), and the transient decay tau (τ) were computed.

Cardiac contractility assessment

Cardiac organoids contractility was measured by video recording of spontaneous beating activity. Organoids were recorded using an EVOS M5000 (ThermoFisher) or EVOS M3000 microscope (ThermoFisher) with 4x or 10x objective. Beating frequency was quantified as beats per minute by manual counting from recorded videos.

RNA-sequencing and data analysis

Immediately after landing, mouse cardiac organoids exposed to parabolic flight conditions and corresponding 1 g ground controls were cryopreserved. For each condition, 36 independent organoids were pooled to generate a single sample. The flight condition comprised organoids collected across three independent parabolic flights (flights 1–3), while the 1g control condition comprised organoids from the corresponding ground control experiments. Total RNA was extracted using NucleoSpin TriPrep kit (Macherey-Nagel) following the manufacturer's instructions. All RNA samples had an RNA integrity number ≥ 7 and concentration ≥ 100 ng/µL (Qubit). cDNA libraries were prepared using cDNA-PCR Sequencing V14-Barcoding kit (SQK-PCB117.24) following the manufacturer's instructions. Briefly, cDNA synthesis was performed using 500ng of total RNA per sample. Following RT, PCR amplification was performed using the following cycling conditions: 1 cycle (95°C for 30 s), 14 cycles (95°C for 15 s, 62°C for 15 s, 65°C for 2 min), 1 cycle (65°C for 6 min). The cDNA libraries were sequenced using a MinION Mk1C sequencing device with R.10.4.1 flow cells for 72h. Reads were aligned to the GRCm39 mouse genome reference with Minimap2 v2.30-r1287[51] and indexed using Samtools 1.22.1[52]. The gene raw counts were generated using FeatureCounts[53] and differential expression analysis was performed using DESeq2[54]. Database for Annotation, Visualization, and Integrated Discovery (DAVID) was used to determine the functional annotations of the top 6 upregulated genes. Search Tool for the Retrieval of Interacting Genes/Protein

(STRING) was used to visualize the interaction network of the top 6 upregulated proteins.

Statistical analysis

All data are presented as mean ± standard deviation. Statistical significance between data were performed with Ordinary one-way ANOVA or Welch's t test using GraphPad Prism 10.6.1 software, with *p-value<0.05, **p-value<0.01, ***p-value<0.001, **** p-value<0.0001. Specific number of independent organoids, experiments and statistical tests are indicated in figure legends.

DATA AVAILABILITY

All data generated or analysed during this study are included in the Source data file.

CODE AVAILABILITY

The underlying codes for this study are not publicly available but may be made available to qualified researchers on reasonable request from the corresponding author.

AUTHOR CONTRIBUTION

E.Y contributed to the conception of the study, the data acquisition, analysis, interpretation of results and drafted the manuscript. H.R was involved in data acquisition, analysis and interpretation of results. F.Y provided guidance through the entire project from the experimental conception to the study execution. C.R developed python AI-based scripts for organoid morphology and calcium fluxes quantification and performed the calcium fluxes analysis. P.G contributed to the data collection, analysis and interpretation of results. C.B. contributed with his expertise in bioinformatic analysis. D.G contributed to the conception and execution of the study. All authors reviewed and approved the manuscript.

ACKNOWLEDGEMENTS

We warmly thank the CNES, and especially G. Gauquelin-Koch, T. Bret-Dibat and S. Rouquette who sponsored our participation in the VP187_69CNES Parabolic Flight campaign. We also thank the Novespace team, in particular Thibault Paris for his guidance for adapting our experiment for parabolic flight. We all thank the entire ALATYR team, especially Guillaume Collange, Mathieu Chaize, Antoine Marin and Flore Bergerot for making this experiment possible. Finally, we thank Pierre-Olivier de Franco from ThermoFisher for lending us an EVOS M3000 through the entire parabolic flight campaign and Chloé Baum from Pasteur Institute Biomics Platform for her advice on the RNA-seq experimental design.

COMPETING INTERESTS

E.Y and D.G are employed by ALATYR but declare no non-financial competing interests. The remaining authors declare no financial or non-financial competing interests.

REFERENCES

1. Vinogradova, O. L., Tomilovskaya, E. S. & Kozlovskaya, I. B. Gravity as a Factor in Evolutionary Adaptation of Animals to Living on the Earth. *Hum. Physiol.* **47**, 716–734 (2021).
2. Bailey, D. M. *et al.* Integrative focus on the space exposome-integrome: physiological challenges and practical limits of countermeasures beyond low Earth orbit. *npj Microgravity* vol. 11 Preprint at https://doi.org/10.1038/s41526-025-00537-1 (2025).
3. Brown, A. H. From gravity and the organism to gravity and the cell. *ASGSB Bull.* **4**, 7–18 (1991).
4. Warthen, K. G. *et al.* Brain and cerebrospinal fluid 3D center of mass shift after spaceflight. *NPJ Microgravity* **11**, (2025).
5. Alzaabi, A. A., Alzaabi, F. M., Siddiqui, R. W., Siddiqui, T. W. & Sami, M. M. Review of microgravity's impact on cardiovascular and nervous systems in space exploration. *npj Microgravity* vol. 11 Preprint at https://doi.org/10.1038/s41526-025-00534-4 (2025).

6. Lee, A. G. *et al.* Spaceflight associated neuro-ocular syndrome (SANS) and the neuro-ophthalmologic effects of microgravity: a review and an update. *npj Microgravity* vol. 6 Preprint at https://doi.org/10.1038/s41526-020-0097-9 (2020).

7. Dontre, A. J. Weighing the impact of microgravity on vestibular and visual functions. *Life Sci. Space Res. (Amst).* **40**, 51–61 (2024).

8. Hupfeld, K. E., McGregor, H. R., Reuter-Lorenz, P. A. & Seidler, R. D. Microgravity effects on the human brain and behavior: Dysfunction and adaptive plasticity. *Neuroscience and Biobehavioral Reviews* vol. 122 176–189 Preprint at https://doi.org/10.1016/j.neubiorev.2020.11.017 (2021).

9. Jordan, J., Limper, U. & Tank, J. Cardiovascular autonomic nervous system responses and orthostatic intolerance in astronauts and their relevance in daily medicine. *Neurological Sciences* vol. 43 3039–3051 Preprint at https://doi.org/10.1007/s10072-022-05963-7 (2022).

10. Sides, M. B. *et al. The Bellagio Report: Cardiovascular Risks of Spaceflight: Implications for the Future of Space Travel*. (2005).

11. Hariom, S. K. & Nelson, E. J. R. Cardiovascular adaptations in microgravity conditions. *Life Sci. Space Res. (Amst).* **42**, 64–71 (2024).

12. Bonanni, R., Cariati, I., Marini, M., Tarantino, U. & Tancredi, V. Microgravity and Musculoskeletal Health: What Strategies Should Be Used for a Great Challenge? *Life* vol. 13 Preprint at https://doi.org/10.3390/life13071423 (2023).

13. Tays, G. D. *et al.* The microgravity environment affects sensorimotor adaptation and its neural correlates. *Cerebral Cortex* **35**, (2025).

14. Lv, H. *et al.* Microgravity and immune cells. *J. R. Soc. Interface* **20**, (2023).

15. Akiyama, T. *et al.* How does spaceflight affect the acquired immune system? *npj Microgravity* vol. 6 Preprint at https://doi.org/10.1038/s41526-020-0104-1 (2020).

16. Hicks, J., Olson, M., Mitchell, C., Juran, C. M. & Paul, A. M. The Impact of Microgravity on Immunological States. https://doi.org/10.4049/immunohorizons.2200063 (2023) doi:10.4049/immunohorizons.2200063.

17. Marchal, S. *et al.* Challenges for the human immune system after leaving Earth. *npj Microgravity* vol. 10 Preprint at https://doi.org/10.1038/s41526-024-00446-9 (2024).

18. Scott, J. M., Stoudemire, J., Dolan, L. & Downs, M. Leveraging Spaceflight to Advance Cardiovascular Research on Earth. *Circulation Research* vol. 130 942–957 Preprint at https://doi.org/10.1161/CIRCRESAHA.121.319843 (2022).

19. Alzaabi, A. A., Alzaabi, F. M., Siddiqui, R. W., Siddiqui, T. W. & Sami, M. M. Review of microgravity's impact on cardiovascular and nervous systems in space exploration. *npj Microgravity* vol. 11 Preprint at https://doi.org/10.1038/s41526-025-00534-4 (2025).

20. Blomqvist, C. G. *et al.* Mechanisms of post-flight orthostatic intolerance. *J. Gravit. Physiol.* **1**, P122-4 (1994).

21. Wnorowski, A. *et al.* Effects of Spaceflight on Human Induced Pluripotent Stem Cell-Derived Cardiomyocyte Structure and Function. *Stem Cell Reports* **13**, 960–969 (2019).

22. Camberos, V. *et al.* The impact of spaceflight and microgravity on the human islet-1+ cardiovascular progenitor cell transcriptome. *Int. J. Mol. Sci.* **22**, (2021).

23. Hwang, H. *et al.* Space microgravity increases expression of genes associated with proliferation and differentiation in human cardiac spheres. *NPJ Microgravity* **9**, (2023).

24. Mair, D. B. *et al.* Spaceflight-induced contractile and mitochondrial dysfunction in an automated heart-on-a-chip platform. *Proc. Natl. Acad. Sci. U. S. A.* **121**, (2024).

25. Shelhamer, M. & Shelhamer, M. HIGHLIGHTED TOPIC Analogs of Microgravity: Space Research without Leaving the Planet Parabolic flight as a spaceflight analog. *J Appl Physiol* **120**, 1442–1448 (2016).

26. Acharya, A. *et al.* Parabolic, flight-induced, acute hypergravity and microgravity effects on the beating rate of human cardiomyo`cytes. *Cells* **8**, (2019).

27. Beckers, F., Seps, B., Ramaekers, D., Verheyden, B. & Aubert, A. E. Parasympathetic heart rate modulation during parabolic flights. *Eur. J. Appl. Physiol.* **90**, 83–91 (2003).

28. Jirak, P. *et al.* Dynamic changes of heart failure biomarkers in response to parabolic flight. *Int. J. Mol. Sci.* **21**, (2020).

29. Lee, J. *et al.* In vitro generation of functional murine heart organoids via FGF4 and extracellular matrix. *Nat. Commun.* **11**, (2020).

30. Lee, J., Ishino, F., Sutani, A. & Kaneko, R. Generation of functional heart organoids from mouse embryonic stem cells. Preprint at https://doi.org/10.21203/rs.3.pex-1078/v1 (2020).

31. Lee, H. A. *et al.* Guidelines for Manufacturing and Application of Organoids: Heart. *Int. J. Stem Cells* **17**, 130–140 (2024).

32. Permyakov, S. E. *et al.* Mouse S100G protein exhibits properties characteristic of a calcium sensor. *Cell Calcium* **87**, (2020).

33. Kimura, Y. *et al.* Changes in the astronaut serum proteome during prolonged spaceflight. *Proteomics* **24**, (2024).

34. Kim, G. S. *et al.* Single-cell analysis identifies Ifi27l2a as a gene regulator of microglial inflammation in the context of aging and stroke in mice. *Nature Communications* **16**, (2025).

35. da Silveira, W. A. *et al.* Comprehensive Multi-omics Analysis Reveals Mitochondrial Stress as a Central Biological Hub for Spaceflight Impact. *Cell* **183**, 1185-1201.e20 (2020).

36. Huang, X., Zhao, S., Hu, M. & Luo, Y. Apolipoprotein M likely extends its anti-atherogenesis via anti-inflammation. *Med. Hypotheses* **69**, 136–140 (2007).

37. Mulari, S. *et al.* Ischemic Heart Disease Selectively Modifies the Right Atrial Appendage Transcriptome. *Front. Cardiovasc. Med.* **8**, (2021).

38. Lin, T. C. Functional roles of spink1 in cancers. *International Journal of Molecular Sciences* vol. 22 Preprint at https://doi.org/10.3390/ijms22083814 (2021).

39. Delp, M. D., Charvat, J. M., Limoli, C. L., Globus, R. K. & Ghosh, P. Apollo lunar astronauts show higher cardiovascular disease mortality: Possible deep space radiation effects on the vascular endothelium. *Sci. Rep.* **6**, (2016).

40. Forghani, P. *et al.* Spaceflight alters protein levels and gene expression associated with stress response and metabolic characteristics in human cardiac spheroids. *Biomaterials* **317**, 123080 (2025).

41. Lecoq, P. E. *et al.* Influence of microgravity on spontaneous calcium activity of primary hippocampal neurons grown in microfluidic chips. *NPJ Microgravity* **10**, (2024).

42. Wnorowski, A. *et al.* Effects of Spaceflight on Human Induced Pluripotent Stem Cell-Derived Cardiomyocyte Structure and Function. *Stem Cell Reports* **13**, 960–969 (2019).

43. Capri, M. *et al.* Long-term human spaceflight and inflammaging: Does it promote aging? *Ageing Research Reviews* vol. 87 Preprint at https://doi.org/10.1016/j.arr.2023.101909 (2023).

44. Versari, S., Longinotti, G., Barenghi, L., Maier, J. A. M. & Bradamante, S. The challenging environment on board the International Space Station affects endothelial cell function by triggering oxidative stress through thioredoxin interacting protein overexpression: the ESA-SPHINX experiment. *The FASEB Journal* **27**, 4466–4475 (2013).

45. Oommen, A. M., Stafford, P. & Joshi, L. Profiling muscle transcriptome in mice exposed to microgravity using gene set enrichment analysis. *NPJ Microgravity* **10**, (2024).

46. Okamura, Y. *et al.* Impact of microgravity and lunar gravity on murine skeletal and immune systems during space travel. *Sci. Rep.* **14**, (2024).

47. Frigeri, A. *et al.* Effect of microgravity on gene expression in mouse brain. *Exp. Brain Res.* **191**, 289–300 (2008).

48. Boerma, M. Space radiation and cardiovascular disease risk. *World J. Cardiol.* **7**, 882 (2015).

49. Shelhamer, M. & Shelhamer, M. HIGHLIGHTED TOPIC Analogs of Microgravity: Space Research without Leaving the Planet Parabolic flight as a spaceflight analog. *J Appl Physiol* **120**, 1442–1448 (2016).

50. Carr, C. E. *et al.* Acceleration profiles and processing methods for parabolic flight. *NPJ Microgravity* **4**, (2018).

51. Li, H. Minimap2: Pairwise alignment for nucleotide sequences. *Bioinformatics* **34**, 3094–3100 (2018).

52. Li, H. *et al.* The Sequence Alignment/Map format and SAMtools. *Bioinformatics* **25**, 2078–2079 (2009).

53. Liao, Y., Smyth, G. K. & Shi, W. FeatureCounts: An efficient general purpose program for assigning sequence reads to genomic features. *Bioinformatics* **30**, 923–930 (2014).

54. Love, M. I., Huber, W. & Anders, S. Moderated estimation of fold change and dispersion for RNA-seq data with DESeq2. *Genome Biol.* **15**, (2014).

Supplementary Files

This is a list of supplementary files associated with this preprint. Click to download.

- SupplementaryMovie2.mp4
- SupplementaryMovie1.mp4
- SupplementaryMovie3.mp4
- SupplementaryMovie4.mp4
- Yamagataetal.2026SourceData.xlsx